The Journal of Chemical Physics ARTICLE scitation.org/journal/jcp

First detection and analysis of an electronic spectrum of vanadium hydride: The $D^5\Pi$–$X^5\Delta$ (0,0) band

Cite as: J. Chem. Phys. 157, 074311 (2022); doi: 10.1063/5.0105844
Submitted: 25 June 2022 • Accepted: 15 July 2022 •
Published Online: 19 August 2022

Thomas D. Varberg[a]

AFFILIATIONS

Department of Chemistry, Macalester College, 1600 Grand Ave., St. Paul, Minnesota 55105, USA

[a]Author to whom correspondence should be addressed: varberg@macalester.edu. Telephone: 651-696-6468

ABSTRACT

The $D^5\Pi$–$X^5\Delta$ (0,0) band of vanadium hydride at 654 nm has been recorded by laser excitation spectroscopy and represents the first analyzed spectrum of VH in the gas phase. The molecules were generated using a hollow cathode discharge source, with laser-induced fluorescence detected via the $D^5\Pi$–$A^5\Pi$ (0,0) transition. All five main ($\Delta\Omega = \Delta\Lambda$) subbands were observed as well as several satellite ones, which together create a rather complex and overlapped spectrum covering the region 15 180–15 500 cm^{-1}. The $D^5\Pi$ state displays the effects of three strong local perturbations, which are likely caused by interactions with high vibrational levels of the $B^5\Sigma^-$ and $c^3\Sigma^-$ states, identified in a previous multiconfigurational self-consistent field study by Koseki *et al.* [J. Phys. Chem. A **108**, 4707 (2004)]. Molecular constants describing the $X^5\Delta$, $A^5\Pi$, and $D^5\Pi$ states were determined in three separate least-squares fits using effective Hamiltonians written in a Hund's case (a) basis. The fine structure of the ground state is found to be consistent with its assignment as a $\sigma\pi^2\delta$, $^5\Delta$ electronic state. The fitted values of its first-order spin–orbit and rotational constants in the ground state are $A = 36.5378(15)$ cm^{-1} and $B = 5.7579(13)$ cm^{-1}, the latter of which yields a bond length of $R_0 = 1.7212(2)$ Å. This experimental value is in good agreement with previous computational studies of the molecule and fits well within the overall trend of decreasing bond length across the series of 3d transition metal monohydrides.

I. INTRODUCTION

The spectroscopy of small, transition metal-containing free radicals has both inspired and confounded experimentalists and theoreticians alike for many years. The $d^n s^2$ and $d^{n+1}s$ configurations of transition metal atoms can produce a multitude of molecular electronic states in the optical region because of the large number of ways the open-shell electrons can be coupled. While many of these states may be dark with respect to the ground state, their presence is felt by their interactions with bright states. Perturbations arise from both homogeneous ($\Delta\Omega = 0$) spin–orbit terms and heterogeneous ($\Delta\Omega = \pm 1$) interactions involving the off-diagonal operators of the rotational Hamiltonian. For transition metal hydrides, in particular, the heterogeneous perturbations can be strong since they scale with the rotational constant, which is an order of magnitude larger than that of a typical non-hydride.

The spectroscopy of transition metal hydrides dates to the 1930s with the pioneering work of Heimer and Heimer on CuH[1] and Gaydon and Pearse on NiH[2] using grating spectrographs. By the end of that decade, the spectra of CrH, MnH, CoH, and ZnH had also been identified and analyzed.[3] Since the 1970s, ScH,[4] TiH,[5] and FeH[6] have been studied spectroscopically, leaving VH as the only remaining first-row transition metal monohydride for which no gas-phase spectral analyses have been reported in the literature.

Here, we present the discovery and analysis of a complex, red-degraded transition of VH at 654 nm, assigned as the (0,0) band of a $^5\Pi$–$^5\Delta$ system and labeled as $D^5\Pi$–$X^5\Delta$. Associated dispersed fluorescence (DF) experiments also revealed the presence of the low-lying $A^5\Pi$ state, and all three electronic states have been characterized by least-squares fitting. Our motivation for finding a spectrum of vanadium hydride arises not only from the paucity of spectroscopic data on the molecule but also from its potential astronomical relevance. Transition metal-containing diatomic molecules are well known in astronomy. For example, the molecules TiO[7] and VO[8] have prominent bands in the spectra of M-type stars, which are useful for temperature profiling studies.[9] In colder L-type stars, TiO

disappears but gets replaced by FeH,[10] CrH,[11] and TiH.[12] These considerations make VH a viable candidate for astronomical detection in cooler stars in our galaxy, so there is a clear need for laboratory studies of VH that could enable astronomical searches for its presence.

The only previous experimental report of an electronic spectrum of VH is a brief description by Smith[13] of weak absorption bands near 470 nm found by shock heating vanadium powder in an argon/hydrogen gas mixture. The bands were recorded using a grating spectrograph and attributed to VH by a comparison with recordings using deuterium in place of hydrogen, but no rotational analysis was attempted. The infrared spectrum of VH trapped in a solid Kr matrix at 12 K has been measured by Xiao *et al.*,[14] who reported the fundamental vibrational transition at 1437.4 cm^{-1} [a value they anticipated will be less than the (unknown) gas-phase value]. The bond dissociation energy of VH has been determined to be $D_0 = 223(7)$ kJ mol^{-1} by guided ion beam mass spectrometry by Armentrout and co-workers.[15,16]

Despite the relative lack of experimental data on the molecule, vanadium hydride has been the subject of ten different *ab initio* calculations dating back to 1974.[17–26] Computational methods for treating electron correlation, spin–orbit coupling, and other relativistic effects have improved considerably in the intervening years, and recent experimental work on TaH[27,28] has shown that the high-level multiconfigurational self-consistent field (MCSCF) calculations of Koseki *et al.*[24] are quite accurate for that molecule. These authors employed two different methods in their calculations, one that utilized an effective core potential (ECP) and the other that used a more expensive all-electron (AE) approach. Both methods included second-order configuration interaction. All three Group 5 metal hydrides VH, NbH, and TaH were studied in Ref. 24, and the present results for VH are compared with this computational study in Sec. V.

II. EXPERIMENTAL DETAILS

Gas-phase VH molecules were produced in a hollow cathode discharge source using a dilute mixture of hydrogen in argon. The gas mixture was flowed through a 2-mm hole in a 6-mm diameter, 10-mm long pure vanadium cathode. A 24-mA direct current electric discharge was maintained via a wire anode located 10 mm from the cathode. The resulting plasma was expanded through a 3-mm wide slit into a vacuum chamber that was pumped to 0.95 Torr. The output from a Coherent 899-29 ring dye laser operating with DCM dye crossed the molecular flow parallel to and 10 mm from the slit. The laser beam was mechanically chopped and multi-passed four times through the gas flow using flat mirrors located outside the chamber. Laser-induced fluorescence was collected and collimated at $f/2$ with a 50-mm diameter lens, focused with another lens into a 1/8-m monochromator (Oriel 77250) at $f/3.7$, detected with a side-on photomultiplier tube (Hamamatsu R-928), and demodulated with an analog lock-in amplifier (Stanford SR510). The monochromator bandwidth was about 18 nm (400 cm^{-1}), and its wavelength was slowly adjusted during laser scanning to pass light 1350 cm^{-1} to the red of the excitation wavenumber, which is where VH fluorescence is at its maximum via the $D^5\Pi \rightarrow A^5\Pi(0,0)$ transition. The use of a monochromator was preferred over just a red-pass optical filter due to the presence of strong interfering lines in the same wavelength region arising from the VO $C^4\Sigma^- - X^4\Sigma^-(0,2)$ and $(1,3)$ bands.[3] Fortuitously, VO fluorescence back to the $v''+1$ and $v''+2$ levels of the $X^4\Sigma^-$ state falls 1000 and 1990 cm^{-1} to the red of the excitation wavenumber, so the monochromator can effectively discriminate against it. The ring laser's onboard wavemeter was calibrated by recording atomic lines of argon optogalvanically using a hollow cathode discharge lamp.[29]

Dispersed fluorescence spectra were recorded at high resolution in order to study the $D^5\Pi \rightarrow A^5\Pi(0,0)$ band in detail. In these experiments, the laser frequency was set to the peak of an individual rotational line. The resulting laser-induced fluorescence was collimated by a lens at $f/2$ and then rotated by 90° with a dove prism so as to focus the light (at $f/6$) onto the vertical entrance slit of a 0.75-m monochromator (Spex 750S). The light was detected with a photomultiplier tube (Hamamatsu R943-02) cooled to −20 °C. With a slit width of 1.0 mm, the bandpass of the monochromator was measured to be about 1.1 nm (FWHM) or ~21 cm^{-1} at the fluorescence wavelength. The monochromator was calibrated by recording the neon emission spectrum from a hollow cathode lamp and generating a linear calibration curve from the known transition wavelengths.[29]

III. APPEARANCE AND ASSIGNMENT OF THE SPECTRUM

A. Laser excitation spectrum of the $D^5\Pi \leftarrow X^5\Delta$ transition

The pursuit of an electronic spectrum of VH was guided by the computational results of Koseki *et al.*,[24] who predicted the strongest transitions in the visible region to be the $F^5\Delta$–$X^5\Delta$ transition at 15 300 cm^{-1} and the $D^5\Pi$–$X^5\Delta$ transition at 12 900 cm^{-1}. An initial search was undertaken that covered the wavenumber range 15 150–16 300 cm^{-1} in the DCM laser dye region. Interference from VO transitions in the same wavelength region was anticipated, so the 1/8-m monochromator used as a bandpass filter was set 1570 cm^{-1} to lower wavenumber of the excitation laser, with the aim of detecting only VH fluorescence. This offset represents the *ab initio* estimate of $\Delta G_{1/2}$ for the $^5\Delta$ ground state. As it turns out, $D^5\Pi$–$X^5\Delta$ (0,1) fluorescence from VH was too weak to be observed, but the $D^5\Pi$ state *does* fluoresce readily to the low-lying $A^5\Pi$ state. Fortuitously, the A state lies 1350 cm^{-1} above the ground state so that a few of the strongest lines of the VH $D^5\Pi \leftarrow X^5\Delta(0,0)$ band were initially discovered by detecting $D^5\Pi \rightarrow A^5\Pi(0,0)$ fluorescence lying at the blue limit of the monochromator's 400 cm^{-1} bandpass.

The D–X (0,0) band of VH covers the wavenumber range 15 180–15 500 cm^{-1}. The system is clearly red-degraded but displays widely spaced rotational lines without much obvious branch structure, owing to the presence of overlapping branches from multiple subbands, which made the rotational analysis challenging. However, the computational work suggested that the transition might be either $^5\Delta_r$–$^5\Delta_r$ or $^5\Pi_r$–$^5\Delta_r$, and a first lines analysis of the rotational branches of the strongest subband, which originates out of the lowest-lying Ω-component of the ground state, revealed the correct assignment as the latter.

If both states in a $^5\Pi$–$^5\Delta$ transition adhere closely to Hund's case (a) coupling, then only five main subbands will be observed,

where the word "main" denotes that $\Delta\Omega = \Delta\Lambda = -1$.[30] Each subband consists of a set of P, Q, and R branches. In the case (a) limit, the projection of J along the internuclear axis is a conserved quantity, which is to say that Ω is a "good" quantum number. However, the $-2B\mathbf{J}\cdot\mathbf{S}$ term in the rotational operator has matrix elements that connect spin–orbit components differing in Ω by ±1, and these spin-uncoupling matrix elements, which are proportional to $-B\sqrt{J(J+1)-\Omega(\Omega\pm1)}\sqrt{S(S+1)-\Sigma(\Sigma\pm1)}$, mix the Ω substates with increasing rotation, causing a transition to a Hund's case (b) energy level pattern. In first row transition metal hydrides, this spin-uncoupling occurs rapidly because the rotational constants are relatively large (~5 cm^{-1}) compared to the separations between adjacent spin–orbit components ($\lesssim$100 cm^{-1}). Furthermore, in states of high multiplicity, the spin-uncoupling occurs faster because the $\sqrt{S(S+1)-\Sigma(\Sigma\pm1)}$ factors are larger. As both the $D^5\Pi$ and $X^5\Delta$ states of VH make transitions to Hund's case (b) coupling with increasing rotation, "satellite" subbands corresponding to $\Delta\Omega = 0$ and +1 transitions become allowed by this mixing. In the VH spectrum, all four of the $\Delta\Omega = 0$ satellite subbands could be tracked starting from their first lines.

The effects of the rapid spin-uncoupling in the two states are also seen in some unusual rotational line spacings at low J, particularly for branches involving the F_3 and F_4 spin components. A dramatic example involves the first four lines in the Q_{43}^{ef} branch, for which $J'' = 2, 3, 4$, and 5. These lie near 15 346.6, 15 333.1, 15 341.9, and 15 349.6 cm^{-1}, resulting in the unexpected pattern of spacings between consecutive members of −13.5, 8.8, and 7.7 cm^{-1}. This unusual behavior can be anticipated for $\Lambda \neq 0$ states of the 3d transition metal hydrides, where the coupling constants $Y = A/B$ are rather small, on the order of 10. Such effects were described in detail by Varberg *et al.*[31] in their analysis of the $A^7\Pi$–$X^7\Sigma^+$ spectrum of MnH.

Figure 1 displays a portion of the VH spectrum near the band origin. The most prominent rotational branch is the Q_1 branch, with its origin near 15 350 cm^{-1}. Subscript 1 identifies the Q_1 branch as belonging to the $^5\Pi_{-1}$–$^5\Delta_0$ subband that involve the lowest energy (F_1) spin components of each state. The Q_1 branch is somewhat stronger than the P_1 branch and about twice as strong as the R_1 branch, a pattern that is consistent with the assignment of a perpendicular transition with $\Delta\Omega = -1$. The Q_1 branch displays well-resolved Λ-doubling, beginning at 0.45 cm^{-1} for $Q_1(1)$ and increasing to 6.15 cm^{-1} for the last assigned member, $Q_1(8)$. A local perturbation occurs at $J' = 5$, where the Λ-doubling drops abruptly in half before growing again. Strong local perturbations are observed in both the $^5\Pi_{-1}$ and $^5\Pi_0$ components of the upper state, and the other three components appear to suffer from smaller perturbations. The ground state shows no signs of any perturbations. As seen in Fig. 1, the five main Q branches are extensively overlapped, which is a consequence of the large rotational spacings and small spin–orbit splittings of the two states.

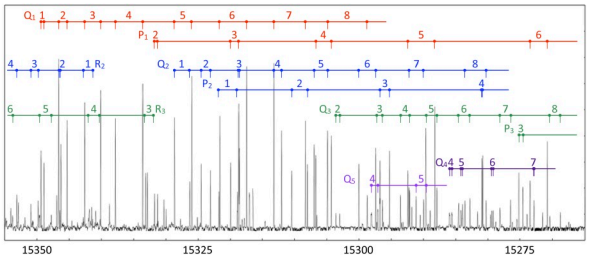

FIG. 1. A portion of the experimental $D^5\Pi$–$X^5\Delta(0,0)$ spectrum near the band origin. All five Q branches of the main ($\Delta\Omega = \Delta\Lambda = -1$) subbands can be observed in this region as well as two R and three P branches. Several satellite ($\Delta\Omega = \Delta\Lambda = 0$ or + 1) Q and P branches also appear but are not labeled to preserve clarity.

The intensities of the main subbands drop off with increasing ground state spin–orbit energy due to the Boltzmann factors, with the highest $^5\Pi_3$–$^5\Delta_4$ subband being about a factor of 10 weaker than the lowest $^5\Pi_{-1}$–$^5\Delta_0$ one. None of the five main R branches forms a head before fading out, and all five branches overlap each other, extending about 30 cm^{-1} to higher wavenumber of the Q_1 origin. Lines belonging to all 15 main rotational branches have been identified, although only the first member of the weak R_5 branch was found.

In addition to the main rotational branches, 10 of the possible 12 $\Delta\Omega = 0$ satellite branches were found, with only the R_{54} and P_{54} branches too weak to be definitively identified. The R_{21}, R_{32}, and R_{43} branches are quite strong—equal to or more intense than the R_1, R_2, and R_3 main branch counterparts. These three satellite branches spread out over more than 100 cm^{-1}, to shorter wavelength of the five main R branches. Furthermore, a weak Q_{21} branch was identified, beginning at $J'' = 2$, despite the fact that such a branch is forbidden in a pure $\Omega = 0 \leftarrow 0$ subband, demonstrating the significant mixing of Ω even at low J. These satellite branches provide direct measures of the spin–orbit splittings in both states, which otherwise can only be determined indirectly via the effects of the spin uncoupling in a pure case (a) $^5\Pi$–$^5\Delta$ transition. A few members of two $\Delta\Omega = +1$ satellite branches (R_{42} and R_{53}) were also found.

The Λ-type doubling in the spectrum arises almost entirely in the upper $^5\Pi$ state, as is anticipated where the lower state is $^5\Delta$. With very few exceptions, this doubling is well resolved for every transition at the Doppler-limited resolution of the experiment. These splittings are unique to each Ω and J level and so proved useful for identifying lines from different branches involving a common upper rotational level, which was critical to assigning the various subbands of the severely overlapped system. The Λ-doubling of the ground $X^5\Delta$ state is three orders of magnitude smaller than that of the upper state. This doubling was critical for making parity assignments for the rotational branches, since the (identical) $R_{ff} - R_{ee}$ and $P_{ff} - P_{ee}$ splitting involving a particular Ω', J' level is slightly different from the $Q_{fe} - Q_{ef}$ splitting.

The upper state vibrational assignment as $v' = 0$ is confirmed by experiments on the isotopologue VD that are currently under way in our laboratory, where the $D^5\Pi$–$X^5\Delta$ (0,0) band has been found with a Q_1 branch origin lying 8 cm^{-1} to higher wavenumber than that of VH. A rotational analysis of the more congested VD spectrum will be reported elsewhere. Furthermore, the highly diagonal character of the $D^5\Pi \rightarrow A^5\Pi$ dispersed fluorescence spectrum (see below), where only a single vibrational band is observed, also supports the assignment of the $D^5\Pi$ vibrational level as $v' = 0$.

Many of the rotational lines involving the F_3, F_4, and F_5 spin components of the two states display a unresolved hyperfine structure, while F_1 and F_2 lines are much narrower. This is not unexpected, since the diagonal matrix element of the hyperfine Hamiltonian in a case (a) basis is proportional to Ω. However, it is perhaps surprising that the hyperfine structure is not fully resolved at the ~0.5 GHz resolution of the experiment, since the ^{51}V nucleus (I = 7/2, 99.7% abundant) has the fourth largest magnetic moment (5.15 μ_N) of all the known nuclides. The relatively narrow hyperfine structure suggests that the 7σ orbital containing an unpaired electron in the ground state (as discussed below) is more V 3dσ than 4s in character, since the significant 4s parentage would introduce a large Fermi contact interaction. Sub-Doppler intermodulated fluorescence experiments are planned to explore the hyperfine structure in detail.

B. Dispersed fluorescence spectrum

Nearly 100 dispersed fluorescence (DF) spectra were recorded on a variety of D ← X excitation transitions accessing all five spin components of the upper state. In this work, the *only* lower state detected in fluorescence was a single vibrational level of a low-lying electronic state, identified as the $A^5\Pi$ (v = 0) level based on the computational results.[17,18,24] A careful search for fluorescence near the excitation wavelength did not reveal evidence of any emission back to the v = 0 level of the $X^5\Delta$ state. Evidently, D → X fluorescence is too weak to be observed at the signal-to-noise ratio of the DF experiments, which was ~10:1 on the strongest D → A features. Some DF scans were recorded out to 930 nm (4600 cm^{-1} to the red of the laser) with the aim of observing fluorescence to either the putative $B^5\Sigma^-$ state or to the v = 1 levels of the $X^5\Delta$ or $A^5\Pi$ states, but none of these were detected.

Fluorescence to the $A^5\Pi(v=0)$ state occurs around 714–718 nm, which places the state 1350 cm^{-1} above the ground state, near the midpoint of the MCSCF predictions of 1792 cm^{-1} (ECP) or 753 cm^{-1} (AE) for the term energy of this state.[24] The observed fluorescence pattern is consistent with a parallel $^5\Pi$–$^5\Pi$ assignment for the transition: a single pair of P–R lines (with $\Omega' = \Omega''$) is found, with a weak Q line present in some cases.[30] Figure 2 presents an example of a DF spectrum displaying one of the strongest Q lines recorded in fluorescence. The measured P–R intervals confirmed assignments in weaker branches of the D–X excitation spectrum, particularly for those out of the $X^5\Delta_3$ and $X^5\Delta_4$ spin–orbit components, since such splittings revealed the value of Ω' and J' of the pump transition via $A^5\Pi$ combination differences determined from preliminary least-squares fitting.

Analysis of the DF spectra revealed a large Λ-doubling in the $A^5\Pi$ state. This doubling provided a way of making absolute parity assignments for the rotational levels of all three observed electronic states in the following manner. In an odd multiplicity Π state, such as $^5\Pi$, Λ-doubling arises from the fact that there exists only one (e or f) parity component of distant $^{2S+1}\Sigma_0$ states that interacts with the same e or f parity component of the $^5\Pi_0$ level, leaving the other $^5\Pi_0$ parity component unaffected. The previous computational studies predict that the nearest Σ state is the $B^5\Sigma^-$ state;[17,18,24] in the MCSCF calculation of Ref. 24, this state is located 950 cm^{-1} (AE) or 2100 cm^{-1} (ECP) above the $A^5\Pi$ state. The next closest Σ state is the $c^3\Sigma^-$ state, computed to be 3000 cm^{-1} (AE) or 5550 cm^{-1} (ECP) above $A^5\Pi$.

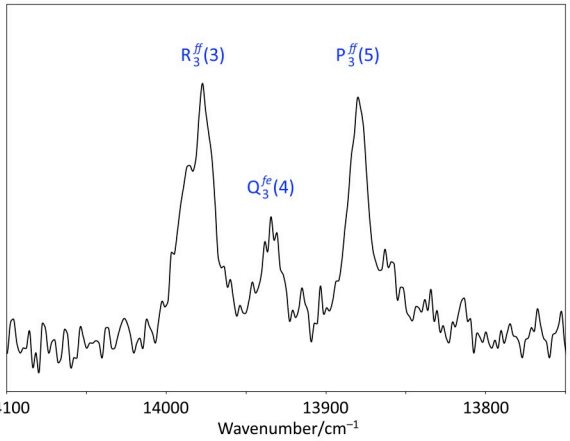

FIG. 2. Dispersed fluorescence spectrum recorded by pumping the $R_{32}^{ff}(3)$ transition of the $D^5\Pi \leftarrow X^5\Delta(0,0)$ band at 15 405.014 cm^{-1}. The three labeled fluorescence peaks are members of the $D^5\Pi \rightarrow A^5\Pi(0,0)$ band.

The $B^5\Sigma_0^-$ component is of f symmetry, while the $c^3\Sigma_0^-$ component is e so that these two higher-lying states will make contributions of opposite sign to the Λ-doubling of the $A^5\Pi$ state.[32] However, the $B^5\Sigma^-$ state is significantly closer in energy, and judging from the calculated potential energy curves,[24] the $B^5\Sigma^-$ and $c^3\Sigma^-$ states should have similar Franck–Condon overlap with the $A^5\Pi$ state. Thus, it is expected that the $B^5\Sigma^-$ state is the predominant source of the $A^5\Pi$ state Λ-doubling, which means the f component will lie below e in the J = 0 level of the $A^5\Pi_0$ state. The parity assignments of the $D^5\Pi \rightarrow A^5\Pi$ dispersed fluorescence spectrum, and consequently those of the $D^5\Pi \leftarrow X^5\Delta$ excitation spectrum, were made in accordance with this expectation.

IV. EXPERIMENTAL RESULTS AND ANALYSIS

A. Energy level expressions

The effective Hamiltonian for the $D^5\Pi$, $A^5\Pi$, and $X^5\Delta$ states was expressed in a Hund's case (a) basis. The Hamiltonian was taken to be

$$H = H_{SO} + H_{rot} + H_{SR} + H_{LD}, \quad (1)$$

where the four operators on the right-hand side represent the spin–orbit, rotational, spin–rotation, and Λ-doubling terms, respectively. An $\mathbf{R}^2$ formalism was employed, in which the rotational operator was written as $B\mathbf{R}^2 = B(\mathbf{J} - \mathbf{L} - \mathbf{S})^2$ and the spin–rotation operator as $H_{SR} = \gamma\mathbf{R}\cdot\mathbf{S}$. These operators have been described by Barnes *et al.*[33] in their work on the $A'^5\Delta$–$X^5\Pi$ transition of CrO, and the exact same forms were used here.

The authors of Ref. 33 included centrifugal distortion terms for the spin–orbit ($A_D, \lambda_D, \eta_D, \theta_D$), rotational ($D$), and Λ-doubling ($D_q, D_{p+2q}, D_{o+p+q}$) terms. For the present work, it was found necessary to add centrifugal distortion terms for the spin–rotation interaction and a higher order centrifugal distortion term for the spin–orbit interaction in both the $D^5\Pi$ and $X^5\Delta$ states, as well as

a set of higher order Λ-doubling centrifugal distortion terms for the $D^5\Pi$ state. The operators describing these interactions were written as

$$H_{\mathrm{SRc.d.}} = \frac{1}{2}\gamma_D\left[\mathbf{R}\cdot\mathbf{S}, \mathbf{R}^2\right]_+, \tag{2}$$

$$H_{\mathrm{SOc.d.}} = \frac{1}{2}A_H\left[L_zS_z, \mathbf{R}^4\right]_+, \tag{3}$$

and

$$H_{\mathrm{LDc.d.}} = \frac{1}{4}H_{o+p+q}\left[S_+^2 + S_-^2, \mathbf{R}^4\right]_+ - \frac{1}{4}H_{p+2q}\left[J_+S_+ + J_-S_-, \mathbf{R}^4\right]_+ + \frac{1}{4}H_q\left[J_+^2 + J_-^2, \mathbf{R}^4\right]_+. \tag{4}$$

Here, the symbol $[x,y]_+$ denotes the anticommutator $xy + yx$, and its use ensures that the matrices are Hermitian. Matrix elements of the effective Hamiltonian were calculated for $^5\Pi$ and $^5\Delta$ states and then compared with those given in Ref. 33 to check for accuracy. The Λ-doubling matrix elements for the $^5\Delta$ state were also compared with the original derivation of such terms by Brown *et al.*,[34] which is also the source of the case (a) notation for these parameters (e.g., $\tilde{n}_\Delta$). Algebraic forms of the matrix elements of the $^5\Delta$ and $^5\Pi$ Hamiltonians are provided in the supplementary material, along with corrections of a few misprints identified in Ref. 33.

B. Least-squares fitting

Three separate least-squares fits to the laser excitation and dispersed fluorescence data were undertaken and are described below using the labels Fit 1, Fit 2, and Fit 3. The results of these fits are summarized in Table I.

(Fit 1—the $X^5\Delta$ state) As previously noted, local perturbations affect many of the rotational levels of the $D^5\Pi$ state, particularly within the $^5\Pi_{-1}$ and $^5\Pi_0$ components. In an initial attempt to fit the D–X spectrum with a single two-state model, it was found that the ground state parameters were significantly contaminated by these upper state perturbations in minimizing the variance of the dataset. Therefore, in Fit 1, molecular constants of the $X^5\Delta$ state were determined separately by fitting data composed of two types of ground state combination differences. (1) For each of the five Ω'' components, first and second rotational combination differences were calculated from pairs of transitions within a subband that terminate on the same upper J and parity level. The Δ_1F combination differences involve R–Q and Q–P pairs, while the Δ_2F values were determined from R–P combinations. Including both first and second combination differences in the dataset appropriately weights the R, Q, and P transitions equally. A total of 159 combination differences were calculated in this way. (2) Ground state spin–orbit intervals were calculated from transitions out of two different $X^5\Delta$ spin components that have a common upper level; an example would be the set of $R_{21}^{ee}(J) - R_2^{ee}(J)$ differences. There are 55 such combination differences in the data.

The results of Fit 1 are listed in the second column of Table I. The 214 data were equally weighted in the least-squares fit, which produced a root-mean-square deviation (RMSD) of 0.0057 cm^{-1}. This RMSD value implies an uncertainty for an individual transition of 0.0040 cm^{-1} (= 0.0057 $cm^{-1}/\sqrt{2}$), which is roughly congruent with our expectations for hyperfine-broadened lines, suggesting that the ground state is modeled within experimental error.

TABLE I. Spectroscopic constants (in cm^{-1}) of the observed electronic states of VH.

	$X^5\Delta$ ($v = 0$)	$A^5\Pi$ ($v = 0$)	$D^5\Pi$ ($v = 0$)
T_0	0.0	1350.16(24)	15 295.229(10)
A	36.5378(15)	38.82(15)	42.2051(74)
A_D	−0.0156(21)	⋯	−0.108 12(91)
10^3A_H	−0.058(10)	⋯	1.888(37)
λ	0.868(15)	0.300(51)	0.3697(25)
$10^3\lambda_D$	−1.07(13)	⋯	⋯
η	0.010 10(65)	0.33(15)	−0.1874(44)
θ	⋯	0.48(11)	⋯
γ	0.908(20)	−0.419(16)	⋯
$10^3\gamma_D$	−0.54(11)	⋯	6.091(95)
B	5.7579(13)	5.866(14)	5.275 78(88)
10^3D	0.2931(26)	0.86(16)	0.104(16)
$10^3\tilde{n}_\Delta$	0.836(19)	⋯	⋯
$10^3\tilde{o}_\Delta$	0.2882(88)	⋯	⋯
$10^3\tilde{p}_\Delta$	0.0308(27)	⋯	⋯
$o + p + q$	⋯	0.479(58)	−0.4927(55)
$p + 2q$	⋯	0.226(22)	0.2124(67)
q	⋯	⋯	0.0059(34)
10^3D_{o+p+q}	⋯	⋯	3.60(50)
10^3D_{p+2q}	⋯	⋯	1.80(37)
10^3D_q	⋯	⋯	0.67(21)
10^3H_{o+p+q}	⋯	⋯	−0.0154(82)
10^3H_{p+2q}	⋯	⋯	−0.0370(50)
10^3H_q	⋯	⋯	−0.0128(34)
Fit no.	Fit 1	Fit 3	Fit 2
N[a]	214	154	194
RMSD[b]	0.0057	0.75	0.0296

[a]Number of data points in the fit.
[b]Root-mean-square deviation (in cm^{-1}) of the unblended lines.

Fitting the four spin–orbit intervals of the $X^5\Delta$ state required both a first-order spin–orbit constant (A) and a spin–spin constant (λ), where the second term is presumably dominated by second-order spin–orbit interactions rather than the diagonal dipolar spin–spin interaction.[31] A third-order spin–orbit term (η) was also well determined in the fit, but the fourth-order parameter θ was not. Centrifugal distortion terms are important in modeling the spectra of metal monohydrides with their large rotational energies, and such corrections were required for the spin–orbit and spin–spin constants as well as the spin–rotation interaction (γ).

The Λ-doubling in a $^5\Delta$ state is expected to be small, since it requires a fourth-order interaction to connect the $|\Lambda = 2\rangle$ and $|\Lambda = -2\rangle$ components through distant Π and Σ states, and this proved to be the case for the $X^5\Delta$ state. Values for the Λ-doubling constants $\tilde{n}_\Delta$, $\tilde{o}_\Delta$, and $\tilde{p}_\Delta$ were determined with relative standard deviations of less than 0.1. All three constants are positive and smaller than 10^{-3} cm^{-1}, making them about three orders of magnitude smaller than the analogous constants in the $D^5\Pi$ state,

confirming that the Λ-doubling observed in the D–X spectrum comes largely from the upper state.

(Fit 2—the $D^5\Pi$ state) With accurate values for the $X^5\Delta$ molecular constants from Fit 1 in hand, the assigned transitions of the D–X excitation spectrum were then fitted by varying only the upper state constants. Given the size of the local perturbations in the $D^5\Pi$ state, it was clear that a meaningful fit required removing the most affected lines from the dataset, resulting in a set of effective constants for the upper state that, it is hoped, are not too different from the true (deperturbed) constants. We chose to exclude from the fit all lines that produced residuals greater than 0.1 cm^{-1}. In successive stages of the fitting, refinement of the constants allowed more lines to be predicted and identified in the spectrum, which were then added to the dataset. The justification for this approach to treating the perturbed D–X spectrum is best demonstrated in Fig. 3, which displays the fitted residuals organized by the upper state spin–orbit component and parity. The effects of local perturbations are clear, particularly for f symmetry levels of the $^5\Pi_{-1}$ and $^5\Pi_0$ spin–orbit components of the D state.

There is a well-known indeterminacy between the γ and A_D parameters in a $^2\Pi$ state that has been described by Brown *et al.*[35] These authors note that this indeterminacy extends approximately to Π states of higher multiplicity, particularly where λ is relatively small in magnitude. In fact, in the $^5\Pi$ Hamiltonian used here, there are six molecular parameters (namely, $B, A_D, \eta_D, \theta_D, \lambda_D$, and γ) available to pin down the five B_Ω values, but only B and A_D were required. If both γ and A_D were floated, it was found that γ was only barely determined (with a relative standard deviation of 0.94), so in the final fit, its value was fixed at zero. This choice did not significantly affect the fitted value of A_D but improved its precision by a factor of 5. The RMSD of Fit 2 is 0.0296 cm^{-1}, nearly an order of magnitude larger than the transition uncertainty of 0.0040 cm^{-1} described previously. This discrepancy reflects the remaining effects of the local perturbations in the upper state.

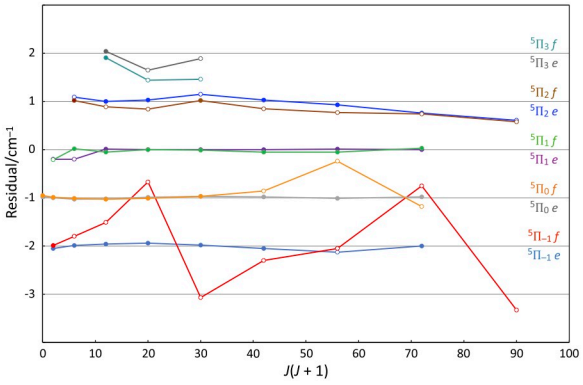

FIG. 3. Fitted residuals of the $D^5\Pi$–$X^5\Delta(0,0)$ band, organized by upper state spin-component and parity. Each datum represents the average residual (observed − calculated wavenumber) of all transitions involving a particular upper rotational level. To displace the plots for purpose of clarity, offsets of −2, −1, 0, 1, and 2 cm^{-1} were added to the residuals of the upper F_1, F_2, F_3, F_4, and F_5 spin components, respectively. Open circles denote transitions that were excluded from the least-squares fit (see text).

(Fit 3—the $A^5\Pi$ state) Given the presence of $D^5\Pi$ state local perturbations, it seemed unwise to fit the $D^5\Pi \rightarrow A^5\Pi$ dispersed fluorescence transitions directly. Instead, a least-squares fit was undertaken that included only A–X energy level differences, which were found in the following manner. For each R, Q, or P line observed in $D^5\Pi \rightarrow A^5\Pi$ dispersed fluorescence, the difference between the excitation and fluorescence wavenumbers was calculated. Each of these values corresponds to an assigned $A^5\Pi$–$X^5\Delta$ energy level difference, and a total of 154 of these differences were fitted. The ground state constants were fixed at the values determined in Fit 1 so that only the $A^5\Pi$ parameters were varied. The spin–orbit intervals of the A state were found to be more asymmetric than those of the X or D states so that a fourth-order spin–orbit parameter was determinable, with a (rather large) fitted value of $\theta = 0.48 \pm 0.11$ cm^{-1}. The $A^5\Pi$ Λ-doubling parameters $o + p + q$ and $p + 2q$ were fitted with relative standard deviations of about 0.1, but a significant value of q could not be determined. Since the fitted standard deviation of q was larger than its magnitude, in the final fit, its value was set to zero.

While individual D ← X excitation wavenumbers are known quite precisely from the calibration of the ring laser, the accuracy of D → A transitions measured in fluorescence is limited by the resolution of the monochromator. For a typical DF transition, the linewidth was found to be ~10 cm^{-1} (FWHM) and the signal-to-noise ratio to be ~10, which together suggest a wavenumber uncertainty of about 1.0 cm^{-1}. The RMSD of Fit 3 is 0.75 cm^{-1}, which indicates that the data are being fitted within their experimental error. The values of the $A^5\Pi$ state constants are shown in the third column of Table I.

V. DISCUSSION

A. Comparing results with previous computational studies

In their MCSCF study, Koseki *et al.*[24] reported term energies for the five spin–orbit components of the ground state using both the ECP and AE approaches. To make an appropriate comparison to the present work, these same term energies for the non-rotating molecule were calculated using the fitted values of A, λ, and η in the ground state. The results are presented in Table II. The ECP method is somewhat more accurate, overestimating the spin–orbit intervals by about 8%, while the AE calculation underestimates them by 16%. Similar results are found for the $A^5\Pi$ state, where the experimental value of the multiplet splitting, $E(^5\Pi_3) - E(^5\Pi_{-1})$, is 156 cm^{-1}. The

TABLE II. Experimental and computational spin–orbit intervals in cm^{-1} for the $X^5\Delta$ state of VH.

Interval	Expt.[a]	ECP[b]	AE[b]
$^5\Delta_1 - ^5\Delta_0$	68	72	53
$^5\Delta_2 - ^5\Delta_1$	71	77	58
$^5\Delta_3 - ^5\Delta_2$	75	81	64
$^5\Delta_4 - ^5\Delta_3$	78	85	71

[a]This work.
[b]Koseki *et al.*[24]

ECP calculation overestimates this splitting by 10%, while the AE method underestimates it by 6%.[36]

The experimental value for the $D^5\Pi$–$X^5\Delta$ transition wavenumber is $\tilde{\nu}_{0,0}$ = 15 295 cm^{-1}. Koseki *et al.*[24] predicted this transition to lie at 12 900 cm^{-1} using the ECP approach, which is an underestimate of 16%. (The Hartree–Fock calculation on VH by Scott and Richards[17] located the $D^5\Pi$ state at 13 970 cm^{-1}.) Koseki *et al.* predict one other allowed transition in the visible region, identified as $F^5\Delta$–$X^5\Delta$ and computed to lie at 15 300 cm^{-1}. This transition was not seen over the extended 15 150–17 650 cm^{-1} search region of the present work.

Most of the previous computational studies on VH have focused on the properties of the four low-lying quintet states of the molecule. In Table III, a comparison is made between the experimental $X^5\Delta$ and $A^5\Pi$ bond lengths and $A^5\Pi$ term energy and those predicted by various computational methods. The fitted rotational constants of the two states yield bond lengths within the $v = 0$ levels of $R_0(X^5\Delta)$ = 1.7212(2) Å and $R_0(A^5\Delta)$ = 1.705(2) Å. These properties were computed at the minima of the potential energy curves in the *ab initio* studies, so for purpose of comparison, equilibrium values were calculated from the spectroscopic $v = 0$ constants using the estimates of α_e, ω_e, and $\omega_e x_e$ from Ref. 24.

It can be seen from Table III that all the Hartree–Fock calculations overestimate the ground state bond length by 0.01–0.09 Å, while the density functional calculations are narrowly spread within ±0.02 Å of the experimental value. The Douglas–Kroll–Hess relativistic treatment (denoted by "-DKH" in Table III) employed in Ref. 26 was found to be quite accurate for other first-row transition metal hydrides as well in the same study. The MCSCF calculations of Koseki *et al.*[24] overestimate the bond length by about 0.05 Å with either the AE or ECP method. The same computational methods were somewhat more accurate for the isovalent TaH molecule.[27]

TABLE III. Experimental and computational properties of VH in its $X^5\Delta$ and $A^5\Pi$ states.[a]

Method	$R_e(X^5\Delta)$	$R_e(A^5\Pi)$	$T_e(A^5\Pi)$	Reference
Experiment[b]	1.704	1.689	1388	This work
DFT/BS-BMK-DKH	1.728			26
DFT/BS-TPSS-DKH	1.681			26
DFT/BS-BMK	1.705			26
DFT/BS-TPSS	1.684			26
DFT/B3LYP/DZP	1.681			22
MCSCF-SOCI/ECP	1.758	1.805	1792	24
MCSCF-SOCI/AE	1.762	1.797	753	24
MCSCF+MCPF	1.719			21
MCSCF+CPF	1.718			21
MCSCF+CISD	1.727			21
MCSCF+CISD	1.74			20
MCSCF	1.74			19
MCSCF	1.76	1.79	2041	18
MCSCF	1.79	1.85	2260	17

[a] R_e denotes the equilibrium bond length in Å, and T_e denotes the term energy in cm^{-1} at the potential minimum.

[b] Experimental equilibrium values were determined from values for $v = 0$ as described in the text.

Experimentally, it is found that the bond length in the $A^5\Pi$ state is 0.015 Å shorter than that of the ground state. This is somewhat surprising given that both states extrapolate to the same V(^{4}F) + H(^{2}S) limit, since a smaller dissociation energy typically implies a weaker and longer bond. None of the three computational studies that computed the $A^5\Pi$ bond length captures this trend.

B. Local perturbations in the $D^5\Pi$ state

There are three strong local perturbations observed in Fig. 3. The $D^5\Pi_{-1}$ component is crossed twice, between $J = 4$ and 5 and again between $J = 8$ and 9, and the $D^5\Pi_0$ component is crossed once, between $J = 7$ and 8. The f symmetry components are perturbed in each case, while the e parity components are not affected. In all three crossings, the perturbing state is one of the lower term energy and with a larger rotational constant. No extra lines could be identified in the neighborhoods of the perturbations.

The fact that only one parity component of the $D^5\Pi$ state is displaced indicates that the perturbers are Σ states. Koseki *et al.*[24] predicted two Σ states below the D state in energy, which are the $B^5\Sigma^-$ state at 1700 cm^{-1} (AE) or 3900 cm^{-1} (ECP) and the $c^3\Sigma^-$ state at 3800 cm^{-1} (AE) or 7600 cm^{-1} (ECP). A $^3\Sigma^-$ state has two e components and one f component[32] so that the $c^3\Sigma^-$ state cannot by itself create these three local perturbations. A $^5\Sigma^-$ state has three f components and two e components. Modeling a case (b) $^5\Sigma^-$ state with a vibrational term energy of 15 090 cm^{-1} and a rotational constant of 4.6 cm^{-1} places the F_5 component at the right energy to cross the $D^5\Pi_{-1}$ substate near $J = 4$ and the $D^5\Pi_0$ substate near $J = 7$. However, the *ab initio* calculation would locate the $v' \approx 10$ level of the $B^5\Sigma^-$ state in the right energy region to intersect with $D^5\Pi(v = 0)$ but with a predicted B value that is much smaller than 4.6 cm^{-1}. Thus, the pattern of the three perturbations cannot be rationalized with a simple, single-state interaction, and it is likely that both the $B^5\Sigma^-$ and $c^3\Sigma^-$ states are involved. Without additional information on the energies of these two states, a more detailed analysis is not possible at this point.

C. Spin–orbit and spin–rotation interactions in the X and A states

Of the first-row transition metals, vanadium has one of the smallest energy gaps between its $4s^13d^{n+1}$ and $4s^23d^n$ configurations, with $E(4s^13d^4) - E(4s^23d^3)$ = 2000 cm^{-1}.[29] The near-degeneracy of the V 4s and 3d orbitals has consequences in the electronic structure of vanadium hydride, where one can expect that both the $4s^13d^{n+1}$ and $4s^23d^n$ configurations of V will contribute to the molecular states. In their complete active space self-consistent field (CASSCF)/CI study of several first-row transition metal hydrides, Walch and Bauschlicher[20] found that the $X^5\Delta$ state of VH represents a mixture of both metal configurations, with a calculated 3d population of 3.42. The ground electronic configuration of the molecule can be written as[17]

$$X^5\Delta : \cdots (6\sigma)^2(7\sigma)^1(3\pi)^2(1\delta)^1. \quad (5)$$

Here, the 6σ orbital is formed from the overlap of a H 1s orbital with a V 4s–3dσ combination, with hydrogen making a larger contribution to this bonding orbital. The 7σ orbital is largely vanadium in character, formed from a mixture of V 4s and 3dσ orbitals. The

3π and 1δ orbitals are nearly pure V 3d orbitals that are essentially non-bonding.

The observed spin–orbit splitting in the $X^5\Delta$ state can be related to the atomic spin–orbit parameters if the single configuration expressed in Eq. (5) is valid. The $X^5\Delta_4$ wavefunction is represented by a single Slater determinant so that the diagonal part of the electron spin–orbit operator is evaluated as[32]

$$\begin{aligned}\langle X^5\Delta_4, \Lambda = +2|\textstyle\sum_i \hat{a}_i l_{iz} s_{iz}|X^5\Delta_4, \Lambda = +2\rangle \\ = \langle \sigma\alpha\pi^+\alpha\pi^-\alpha\delta^+\alpha|\textstyle\sum_i \hat{a}_i l_{iz} s_{iz}|\sigma\alpha\pi^+\alpha\pi^-\alpha\delta^+\alpha\rangle \\ = 2\cdot\frac{1}{2}\langle\delta|\hat{a}|\delta\rangle = a_\delta. \end{aligned} \tag{6}$$

Equating this result to the spin–orbit matrix element from Eq. (1), $\langle {}^5\Delta_4|H_{SO}|{}^5\Delta_4\rangle = 4A$, one obtains $A(X^5\Delta) = (1/4)a_\delta$. If the 1δ orbital is a pure V 3d orbital, then a_δ should equal the atomic spin–orbit parameter ζ_{3d}. Dunn[37] has found that $\zeta_{3d} = 130\ cm^{-1}$ for $V(3d^4 4s)$ and $160\ cm^{-1}$ for $V(3d^3 4s^2)$, from fitting experimental atomic data. The calculated molecular 3d population of 3.42 suggests that $\zeta_{3d} \approx 145\ cm^{-1}$ is appropriate for VH. With this value, the $X^5\Delta$ spin–orbit constant is predicted to be $A = 36.2\ cm^{-1}$, which is in good agreement with the fitted value $A = 36.538(2)\ cm^{-1}$.

Scott and Richards[17] wrote the $A^5\Pi$ state as a mixture of $(7\sigma)^1(3\pi)^1(1\delta)^2$ and $(7\sigma)^1(8\sigma)^1(1\pi)^1(1\delta)^1$ configurations, abbreviated as

$$A^5\Pi : \alpha|\sigma\pi\delta^2| + \beta|\sigma\sigma'\pi\delta|. \tag{7}$$

They estimated the values $\alpha = 0.82$ and $\beta = 0.57$ by a configuration interaction calculation. Such a description leads to a result similar to Eq. (6),

$$\begin{aligned}\langle A^5\Pi_3, \Lambda = +1|\textstyle\sum_i \hat{a}_i l_{iz} s_{iz}|A^5\Pi_3, \Lambda = +1\rangle \\ = \alpha^2\left(\frac{1}{2}a_\pi\right) + \beta^2\left(-\frac{1}{2}a_\pi + a_\delta\right) = \frac{1}{2}\zeta_{3d} \end{aligned} \tag{8}$$

where $a_\pi = a_\delta = \zeta_{3d}$. The cross-terms in Eq. (8) vanish because the one-electron spin–orbit operator does not act between σ and δ orbitals. Since $\langle {}^5\Pi_3|H_{SO}|{}^5\Pi_3\rangle = 2A$, then $A(A^5\Pi) = 36.2\ cm^{-1}$, as was obtained for the $X^5\Delta$ state. Again, this agrees reasonably well with the fitted value of $A = 38.82(15)\ cm^{-1}$.

The well-determined spin–rotation parameters in the X and A states are surprisingly large: $\gamma(X^5\Delta) = 0.91(2)\ cm^{-1}$ and $\gamma(A^5\Pi) = -0.42(2)\ cm^{-1}$. The value of γ in an electronic state is the sum of the first-order spin–rotation interaction, $\gamma^{(1)}$, which is expected to be small in size, and the contributions that arise in second order from spin–orbit interactions with distant states.[35] For the ground $^5\Delta$ state, only $^5\Pi$ and $^5\Phi$ states can contribute to $\gamma^{(2)}$. We can estimate $\gamma^{(2)}$ in the usual manner, using the appropriate expression found in Table I of Ref. 35, if we assume that the X and A states are described by configurations (5) and (7) and that the $A^5\Pi(v = 0)$ level is the sole source of the second-order interaction in the $X^5\Delta$ state. Taking $\langle B(r)\rangle = 5.58\ cm^{-1}$ (the average of the two *B*-values), $\zeta_{3d} = 145\ cm^{-1}$, and $E(^5\Delta) - E(^5\Pi) = -1350\ cm^{-1}$ yields an estimate of $\gamma^{(2)} = 1.20\ cm^{-1}$, which is in reasonably good agreement with the fitted value $\gamma(X^5\Delta) = 0.91\ cm^{-1}$. The overestimation might reflect the fact that the more distant $A^5\Pi(v = 1)$ level will also contribute, which when taking account of the vibrational overlap factors will decrease the value of $\gamma^{(2)}$. An analogous *a priori* estimate of $\gamma^{(2)}$ in the $A^5\Pi$ state is more complicated, since its $v = 0$ level likely lies in between the $v = 0$ and 1 levels of the $X^5\Delta$ state. The fact that the observed $\gamma(A^5\Pi) < 0$ suggests that the second-order interaction with the $v = 0$ level of the ground state dominates over that with the $v = 1$ level, presumably on account of a larger vibrational overlap integral.

D. Lambda-doubling in the $A^5\Pi$ and $D^5\Pi$ states

As described earlier in Sec. III B, the Λ-doubling in the $A^5\Pi$ state is expected to be determined mostly by its interaction with the $B^5\Sigma^-$ state, with a smaller contribution from the more distant $c^3\Sigma^-$ state. In Fit 3 of the $A^5\Pi$ state, only the two Λ-doubling parameters $o + p + q$ and $p + 2q$ could be determined, with *q* being fixed to zero. The fitted values of these constants yield $o = 0.253\ cm^{-1}$, $p = 0.226\ cm^{-1}$, and $q = 0$. Estimating second-order values for these parameters (using the expressions in Table II of Ref. 35) is complicated by the fact that the A and B states are not well represented by single configurations. Bearing this caveat in mind, if one assumes that the dominant configurations of the two states are $(7\sigma)^1(3\pi)^1(1\delta)^2$, $A^5\Pi$ and $(7\sigma)^1(1\delta)^2(8\sigma)^1$, $B^5\Sigma^-$ and that the Λ-doubling in the $A^5\Pi$ state is determined solely by second-order interactions with $B^5\Sigma^-(v = 0)$, then taking the values $\langle B\rangle(r) = 5.87\ cm^{-1}$, $\zeta_{3d} = 145\ cm^{-1}$, and $E(^5\Pi) - E(^5\Sigma^-) = -2000\ cm^{-1}$ (which is the MCSCF ECP estimate[24]) produces a value for the parameter $p = (1.28\alpha^2)\ cm^{-1}$, where α^2 is the fractional V 3dσ character of the 8σ orbital. The fitted value of $p = 0.226\ cm^{-1}$ is obtained if α^2 is chosen to be 0.18. Similarly, it is found that $q = (0.21\alpha^2)\ cm^{-1}$, which for the same choice of α^2 yields a second-order estimate for *q* of $0.037\ cm^{-1}$. This estimated value is a factor of six smaller than that of *p*, which may explain why *q* could not be determined in the least-squares fit. Finally, the second-order contribution to the parameter *o* is calculated to be of positive sign, which agrees with the sign of the fitted value. While these second-order estimates are only rough approximations, especially since the location of the $B^5\Sigma^-$ state is not known experimentally, they do lend support to the hypothesis that $B^5\Sigma^-$ state interactions in second order are the dominant source of Λ-doubling in the $A^5\Pi$ state.

Identifying the sources of Λ-doubling in the $D^5\Pi$ state is much more complicated, since this state is located among high vibrational levels of both the $B^5\Sigma^-$ and $c^3\Sigma^-$ states. A plot of the calculated Λ-doublings against *J* for the $D^5\Pi$ state is displayed in Fig. 4. Analogous Λ-doubling plots for the X and A states are included in the supplementary material.

E. First-row transition metal hydrides

This work presents the first analysis of a gas-phase spectrum of vanadium hydride, so there now exist spectroscopic data on all ten first-row transition metal monohydrides (or more correctly, the 3d block metal monohydrides, since zinc is not usually defined to be a transition metal). Thus, we are in a good position to consider trends across the 3d transition series.

The bonding in these molecules can be broadly described as follows: Three σ molecular orbitals are formed from a basis consisting of the metal (M) 4s and 3dσ orbitals and the H 1s orbital. The

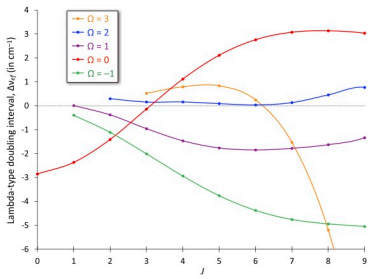

FIG. 4. Calculated Λ-type doubling intervals for the $D^5\Pi$ state of VH, defined as $\Delta\nu_{ef}(J) = F_e(J) - F_f(J)$.

lowest of these is the 6σ (bonding) orbital, which is mostly hydrogenic in character, giving the molecule significant M^+H^- character when it is filled with two electrons. As Z_{eff} increases across the row, the ionization potential of the metal increases. This, in turn, lowers the energies of the metallic 3d and 4s orbitals, giving the 6σ orbital increasing M character. The 7σ orbital is mostly metallic in character and is polarized away from the $H^{\delta-}$ end of the molecule. The (typically empty) 8σ orbital is partially antibonding and will also have a significant contribution from M 4pσ.[31] The other valence molecular orbitals are the (nonbonding) 3π and 1δ orbitals, which are formed from M 3d orbitals.

In every case, the 6σ orbital contains two electrons. The ground state of ScH is $(6\sigma)^2(7\sigma)^2, {}^1\Sigma^+$. In the next four molecules—TiH, VH, CrH, and MnH—only one electron is placed in the 7σ orbital, with the remaining electrons going into the 3π and 1δ orbitals, arranged in a high-spin configuration. In FeH, the 7σ orbital again contains two electrons, with successive electrons placed in the 3π and 1δ orbitals.

Table IV lists the term symbols, spectroscopic properties, and electronic configurations of the ground states of the ten monohydrides. The observed trend in the bond length across the series agrees with the general features described above. Molecular bond lengths, broadly speaking, reflect both the size of the atomic valence orbitals and the strength of the chemical bond that is formed. As seen in Table IV, as one moves across the 3d row, the bond length monotonically decreases with only two exceptions, which are MnH and ZnH. In MnH, a single electron is placed in the partially antibonding 8σ orbital in order to preserve the unusually stable Mn $3d^5(\sigma\pi^2\delta^2)$ configuration, while in ZnH, an electron is placed in this orbital because the 3d subshell is completely full. For both these outliers, the bond length is more than 0.1 Å longer than the value predicted from the overall trend. The vibrational frequency, tabulated in the table as the wavenumber of the lowest vibrational interval, rises across the series. Since the reduced masses of the hydrides are all very close to 1.0, these intervals effectively scale with the square root of the force constant and so reflect an increase of the chemical bond strength across the series. Again, the two most obvious exceptions to this trend are MnH and ZnH.

VI. CONCLUSION

We report the first analysis of a gas-phase spectrum of VH, assigned as the (0,0) band of the $D^5\Pi$–$X^5\Delta$ electronic transition. The spectrum covers the 15 180–15 500 cm^{-1} region and is rather complex in appearance, with many overlapping subbands. In addition to identifying all 15 main ($\Delta\Omega = -1$) branches, 10 of the possible 12 branches with $\Delta\Omega = -1$ and two of the possible nine branches with $\Delta\Omega = 1$ were also observed. These latter satellite branches are induced by the rapid spin-uncoupling that occurs in both electronic states. Molecular constants for the two states were determined by least-squares fitting using effective Hamiltonians written in a Hund's case (a) basis. The ground state was fitted separately to insulate against the effects of several local perturbations in the upper state. The strength of the transition is rather weak, with dispersed fluorescence experiments revealing measurable fluorescence only to the $v = 0$ vibrational level of the low-lying $A^5\Pi$ state. Rotational analysis of this fluorescence permitted a determination of the principal molecular constants of the $A^5\Pi$ state as well.

TABLE IV. The ground states of the 3d transition metal monohydrides.[a]

Molecule	Ground state	$\Delta G_{1/2}$ (cm^{-1})	B_0 (cm^{-1})	R_0 (Å)	Electronic configuration	References
ScH	$^1\Sigma^+$	1546.973	5.363 03	1.7857	σ^2	38
TiH	$^4\Phi$	1520	5.362 06	1.7847	σπδ	39 and 41
VH	$^5\Delta$	⋯	5.757 9	1.7212	$\sigma\pi^2\delta$	This work
CrH	$^6\Sigma^+$	1581.2	6.131 741	1.6676	$\sigma\pi^2\delta^2$	3 and 41
MnH	$^7\Sigma^+$	1490.4	5.605 75	1.7432	$\sigma\pi^2\delta^2\sigma'$	3 and 31
FeH	$^4\Delta$	1762.94	6.484 82	1.6204	$\sigma^2\pi^2\delta^3$	6
CoH	$^3\Phi$	⋯	7.136 3[b]	1.5440[b]	$\sigma^2\pi^3\delta^3$	42
NiH	$^2\Delta$	1927.6845	7.753 02	1.4815	$\sigma^2\pi^4\delta^3$	43
CuH	$^1\Sigma^+$	1866.4093	7.817 333 5	1.4744	$\sigma^2\pi^4\delta^4$	44 and 45
ZnH	$^2\Sigma^+$	1496.4779	6.547 631	1.6109	$\sigma^2\pi^4\delta^4\sigma'$	46

[a]Values of the first vibrational interval ($\Delta G_{1/2}$) and the rotational constant and bond length within the $v = 0$ level (B_0 and R_0) are listed for the isotopologue containing the most abundant metal isotope.
[b]Value within the lowest Ω-component ($^3\Phi_4$) of the ground state.

The bond length of the molecule predicted using density functional theory by other workers is found to be in close agreement with the experimental value determined here, while Hartree–Fock methods modestly overestimate it. None of the previous calculations predict the observed shortening of the bond in the $A^5\Pi$ state. Vanadium hydride is the last of the 3d transition metal monohydrides for which there are no analyzed spectra of the molecule in the gas phase. The results presented here begin to fill in this spectroscopic blank. They may also prove useful for astronomical detection of VH in colder stars within our galaxy.

SUPPLEMENTARY MATERIAL

See the supplementary material for tables of the observed and calculated wavenumbers of the D–X spectrum, the datasets used for Fits 1 and 3, the calculated energy levels of all three fitted states, and the calculated transition frequencies of the pure rotational spectrum of VH in its ground state. Figures displaying the Λ-type doubling intervals within the $X^5\mathbf{\Delta}$ and $A^5\mathbf{\Pi}$ states are included, and the matrix elements of the $^5\mathbf{\Delta}$ and $^5\mathbf{\Pi}$ Hamiltonians are also listed.

ACKNOWLEDGMENTS

This material is based upon work supported by the National Science Foundation under Grant No. CHE-2100542.

AUTHOR DECLARATIONS

Conflict of Interest

The author has no conflicts to disclose.

Author Contributions

Thomas D. Varberg: Conceptualization (lead); Data curation (lead); Formal analysis (lead); Funding acquisition (lead); Investigation (lead); Methodology (lead); Project administration (lead); Resources (lead); Software (lead); Validation (lead); Visualization (lead); Writing – original draft (lead); Writing – review & editing (lead).

DATA AVAILABILITY

The data that support the findings of this study are available within the article and its supplementary material.

REFERENCES

[1]A. Heimer and T. Heimer, Z. Phys. **84**, 222 (1933).
[2]A. G. Gaydon and R. W. B. Pearse, Nature **134**, 287 (1934).
[3]K. P. Huber and G. Herzberg, *Molecular Spectra and Molecular Structure IV. Constants of Diatomic Molecules* (Van Nostrand Reinhold, New York, 1979).
[4]A. Bernard, C. Effantin, and R. Bacis, Can. J. Phys. **55**, 1654 (1977).
[5]A. G. Gaydon, J. Phys. B: At., Mol. Opt. Phys. **7**, 2429 (1974).
[6]J. G. Phillips, S. P. Davis, B. Lindgren, and W. J. Balfour, Astrophys. J., Suppl. Ser. **65**, 721 (1987).
[7]F. Azizi and M. T. Mirtorabi, Astrophys. Space Sci. **357**, 96 (2015).
[8]J. D. Kirkpatrick, Annu. Rev. Astron. Astr. **43**, 195 (2005).
[9]P. F. Bernath, Int. Rev. Phys. Chem. **28**, 681 (2009).
[10]R. P. Schiavon, B. Barbuy, and P. D. Singh, Astrophys. J. **484**, 499 (1997).
[11]J. D. Kirkpatrick, I. N. Reid, J. Liebert, R. M. Cutri, B. Nelson, C. A. Beichman, C. C. Dahn, D. G. Monet, J. E. Gizis, and M. F. Skrutskie, Astrophys. J. **519**, 802 (1999).
[12]A. Burrows, M. Dulick, C. W. Bauschlicher, Jr., P. F. Bernath, R. S. Ram, C. M. Sharp, and J. A. Milsom, Astrophys. J. **624**, 988 (2005).
[13]R. E. Smith, Proc. R. Soc. London, Ser. A **332**, 113 (1973).
[14]Z. L. Xiao, R. H. Hauge, and J. L. Margrave, J. Phys. Chem. **95**, 2696 (1990).
[15]Y. M. Chen, D. E. Clemmer, and P. B. Armentrout, J. Chem. Phys. **98**, 4929 (1993).
[16]L. Cheng, J. Gauss, B. Ruscic, P. B. Armentrout, and J. F. Stanton, J. Chem. Theory Comput. **13**, 1044 (2017).
[17]P. R. Scott and W. G. Richards, J. Phys. B: At., Mol. Opt. Phys. **7**, L347 (1974).
[18]G. A. Henderson, G. Das, and A. C. Wahl, J. Chem. Phys. **63**, 2805 (1975).
[19]G. Das, J. Chem. Phys. **74**, 5766 (1981).
[20]S. P. Walch and C. W. Bauschlicher, Jr., J. Chem. Phys. **78**, 4597 (1983).
[21]D. P. Chong, S. R. Langhoff, C. W. Bauschlicher, Jr., S. P. Walch, and H. Partridge, J. Chem. Phys. **85**, 2850 (1986).
[22]V. Barone and C. Adamo, Int. J. Quantum Chem. **61**, 443 (1997).
[23]J. F. Harrison, Chem. Rev. **100**, 679 (2000).
[24]S. Koseki, Y. Ishihara, D. G. Fedorov, H. Umeda, M. W. Schmidt, and M. S. Gordon, J. Phys. Chem. A **108**, 4707 (2004).
[25]F. Furche and J. P. Perdew, J. Chem. Phys. **124**, 044103 (2006).
[26]S. Goel and A. E. Masunov, J. Chem. Phys. **129**, 214302 (2008).
[27]S. P. Gleason, D. H. P. Kellett, P. P. Reischmann, and T. D. Varberg, J. Mol. Spectrosc. **362**, 56 (2019).
[28]Z. T. P. Fried, S. Singh, and T. D. Varberg, J. Mol. Spectrosc. **372**, 111332 (2022).
[29]National Institute of Standards and Technology, Physical Measurement Laboratory, Atomic Spectra Database, 2020, https://physics.nist.gov/asd/; accessed July 2020.
[30]G. Herzberg, *Molecular Spectra and Molecular Structure: I. Spectra of Diatomic Molecules*, 2nd ed. (Van Nostrand, New York, 1950).
[31]T. D. Varberg, J. A. Gray, R. W. Field, and A. J. Merer, J. Mol. Spectrosc. **156**, 296 (1992).
[32]H. Lefebvre-Brion and R. W. Field, *The Spectra and Dynamics of Diatomic Molecules* (Elsevier, Amsterdam, 2004).
[33]M. Barnes, P. G. Hajigeorgiou, and A. J. Merer, J. Mol. Spectrosc. **160**, 289 (1993).
[34]J. M. Brown, A. S.-C. Cheung, and A. J. Merer, J. Mol. Spectrosc. **124**, 464 (1987).
[35]J. M. Brown, E. A. Colbourn, J. K. G. Watson, and F. D. Wayne, J. Mol. Spectrosc. **74**, 294 (1979).
[36]The $A^5\mathbf{\Pi}$ multiplet splittings were estimated as 172 cm^{-1} (ECP) and 146 cm^{-1} (AE) by inspection of the plotted potential energy curves in Figs. 1 and 1S of Ref. 24.
[37]T. M. Dunn, Trans. Faraday Soc. **57**, 1441 (1961).
[38]R. S. Ram and P. F. Bernath, J. Chem. Phys. **105**, 2668 (1996).
[39]C. Linton, T. C. Steimle, and S. E. Frey, J. Mol. Spectrosc. **279**, 1 (2012).
[40]O. Launila and B. Lindgren, J. Chem. Phys. **104**, 6418 (1996).
[41]R. S. Ram, C. N. Jarman, and P. F. Bernath, J. Mol. Spectrosc. **161**, 445 (1993).
[42]T. D. Varberg, E. J. Hill, and R. W. Field, J. Mol. Spectrosc. **138**, 630 (1989).
[43]T. Nelis, S. P. Beaton, K. M. Evenson, and J. M. Brown, J. Mol. Spectrosc. **148**, 462 (1991).
[44]J. Y. Seto, Z. Morbi, F. Charron, S. K. Lee, P. F. Bernath, and R. J. Le Roy, J. Chem. Phys. **110**, 11756 (1999).
[45]T. D. Varberg and K. M. Evenson, J. Mol. Spectrosc. **164**, 531 (1994).
[46]A. Shayesteh, R. J. Le Roy, T. D. Varberg, and P. F. Bernath, J. Mol. Spectrosc. **237**, 87 (2006).